1 IXS: INELASTIC SCATTERING BEAMLINE

1.1 Executive Summary

We present in this chapter a preliminary design of the Inelastic X-ray Scattering (IXS) beamline for NSLS-II. The scientific objective of the beamline is focused on very high-resolution (1 meV ~ 0.1 meV) IXS experiments as outlined in the NSLS-II Conceptual Design Report delivered in December 2006. The NSLS-II User Workshop in July 2007 provides further inputs from the user community on the scientific drivers for this beamline. The beamline as designed includes two endstations, one with 1meV and the other with 0.1meV energy resolution, both of which take full advantage of the high brightness and flux of the NSLS-II source at ~10 keV. To achieve the 0.1meV resolution goal for NSLS-II, the current design employs a newly proposed scheme based on highly asymmetrically cut Si crystal optics operating at exact back-scattering. This novel approach, albeit yet to be demonstrated in a working device for which active R&D are required, provides a unique opportunity for NSLS-II to build a fundamentally new instrument with unprecedented performance for inelastic x-ray scattering experiments that are not yet feasible on any existing instruments to date.

The scope of the present document includes the scientific objective, the radiation source, the overall beamline layout, rationales for beamline optics, the power management and the expected performance. Some design details will be presented, including the beamline vacuum system, data acquisition and motion control, and beamline components that are likely to remain the same regardless the details of the endstation design. Details on the Personnel Safety System, the Equipment Protection System, as well as additional requirements on the conventional facilities and accelerator systems will also be discussed.

Several possible configurations of the 1meV endstation will be outlined. One will be based on the same scheme as that for the 0.1meV endstation, but optimized to operate at 1meV energy resolution. This would be a logical choice as demonstrating the scheme for achieving the 0.1meV energy resolution works for 1 meV is a milestone of its own. Others are based on existing experience in building IXS beamlines that offer 1meV energy resolution at ESRF, SPring-8 and APS using Si crystal optics operating at higher photon energies. The intension here is to use crystals of lower symmetry such as quartz or sapphire which offer many possible choices of refraction with intrinsic width of the order of 1 meV at energies ~10 keV. There are concerns regarding the quality of these crystals for use as high-resolution x-ray optics. There are however substantial efforts now in making better crystals at several groups around the world. We will monitor the progress of those efforts and make a decision on the configuration of the 1meV endstation at some point in future.

The total estimated cost of the beamline based on the details of the current design stands at $9.915M, which includes the enclosures, beam transport, utilities, white beam components, high heatload optics, beam conditioning optics, Personnel Safety System, Equipment Protection System, beamline controls, and project management. The cost for the 0.1meV endstation is also included.

Finally, we would like to emphasize that the present design is still at a very preliminary stage. The final design of the beamline as well as the endstations will largely depend on the final technical details for achieving the 0.1meV energy resolution, where an active R&D program will be required and pursued. The design process will further involve consultations with the user community through workshops and with the Beamline Advisory Team (BAT) in the coming years, whereby the scientific focus of the beamline and endstations and hence their design will be further refined.

1.2 Scientific Objective

Inelastic X-ray Scattering is a momentum-resolved technique for studying dynamics and excitations in condensed matter systems. The scientific objective of the present IXS beamline is focused on very high-resolution (1 meV ~ 0.1 meV) IXS experiments for studying low-energy dynamics of a variety of systems. The NSLS-II User Workshop in July 2007 (see the breakout session on inelastic x-ray scattering at the following link: http://www.bnl.gov/nsls2/workshops/UserWorkshop_BOS2.asp) further identifies a few key scientific drivers for this beamline. They are grouped into several classes of experiments according to the required energy resolution:

- 0.1meV resolution experiments
  Examples include visco-elastic crossover behaviors of disordered systems and fluids, and new low-energy modes in complex fluids and confined systems that would require the 0.1meV resolution to be resolved. Another important area of research is in the collective dynamics of lipid membranes and other biological systems, where correlated molecular motions and density fluctuations on the meV energy scale play a significant role in determining their physical properties. The 0.1meV resolution would also be potentially useful for mapping the superconducting band gap with phonons.
- 1meV resolution experiments
  Examples include relaxation processes in disordered systems such as glasses, fluids, polymers, etc. The higher available flux promised by NSLS-II compared to existing instruments will be highly valuable for studying phonons in single crystals, surfaces, thin films, small samples down to micrometer sizes, systems under extreme pressure, phonons in excited states (pump probe), and exotic excitations in strongly correlated systems.

It is clearly recognized by the community that the 0.1meV endstation should be designed to bridge, at least partially, the dynamic gap between existing high- and low-frequency probes, which would enable new science to be done. The most exciting scientific problems requiring this energy resolution are envisaged to come from disordered systems in the forward scattering direction, where very high momentum resolution (<0.1 nm^{-1}) would also be required. For the 1meV resolution experiments, the higher available flux promised by NSLS-II should allow studies ranging from phonons in small single crystals, surfaces, thin films, to exotic excitations in strongly correlated materials, where the range of momentum transfer should cover typical Brillouin zone sizes. To take full advantage of the superior performance at ~10 keV of the NSLS-II source, the requirements and specifications for the beamline and endstations include:

- The primary beam energy is chosen at 9.1 keV near the peak of the tuning curve of a U19 undulator and also to match the proposed scheme for achieving the 0.1meV energy resolution. This energy should however be tunable over 7 ~ 12 keV to retain certain flexibility in case a different choice of refraction may be required.
- Due to the different experimental requirements for 0.1meV and 1meV resolution, there should be two endstations, one optimized for the 0.1meV, and the other for the 1meV experiments.
- The energy scan range should be on the order of 100 meV for the 0.1meV endstation, and up to about 1 eV for the 1meV endstation.
- Momentum resolution should be better than 0.1 nm^{-1} at low momentum transfer. This corresponds to an angular acceptance of less than 10 mrad for the analyzer at 9.1 keV.
- For the 1meV endstation, the momentum scan range should be up to 80 nm^{-1} in order to cover typical Brillouin zone sizes of small single crystals. This translates to a scattering angle of 120 deg at 9.1 keV.
- Beam spot size should be ≤ 5 μm (V) × 10 μm (H). This would enable studies of very small samples and samples under extreme pressure generated using diamond anvil cells.

1.3 Insertion Device

Inelastic x-ray scattering is a photon-hungry experiment. The figure-of merit for a radiation source for an IXS beamline is therefore the flux (photons per second per meV) that it delivers to the sample. The brightness or the ultimate beam spot size on the sample becomes secondary in this case, so long as it suffices to achieve the required energy resolution and be compatible with the required sample environments such as for extreme pressure. Of the devices considered in the baseline of NSLS-II, a 3m-long U19 undulator offers the best performance over 7 ~ 12 keV. Key parameters of the U19 undulator are summarized in Table 1.1.

Table 1.1. Basic parameters of a U19 undulator.

IVU specs	U19
Device type	CPMU / in vacuum
Peak field	1.14 T
Lowest 3rd harmonic energy for 3.0 GeV beam	4.4 keV
Highest harmonic to be used	7
Maximum K value – corresponding to the lowest third harmonic energy	2.03
Overall length of magnet array	3 m
Period	19 mm
Minimum magnet gap	5 mm

For further improvements that could lead to a significant increase of the incident flux, one of the options being considered is placing multiple undulators in a single long straight section. Possible choices include two 3m-long U19 or three 2m-long U14 undulators. A five-fold increase of flux is expected, for example, by using three 2m-long superconducting undulators (SCU) U14 instead of a single 3m U19 device (Figure 1.1). This assumes the ability to refocus the beam between such devices, which requires careful studies of the accelerator systems during the design phase. If the issue of refocusing can be resolved, it is obvious that the IXS beamline could make a perfect case for yet an even longer straight section for more devices.

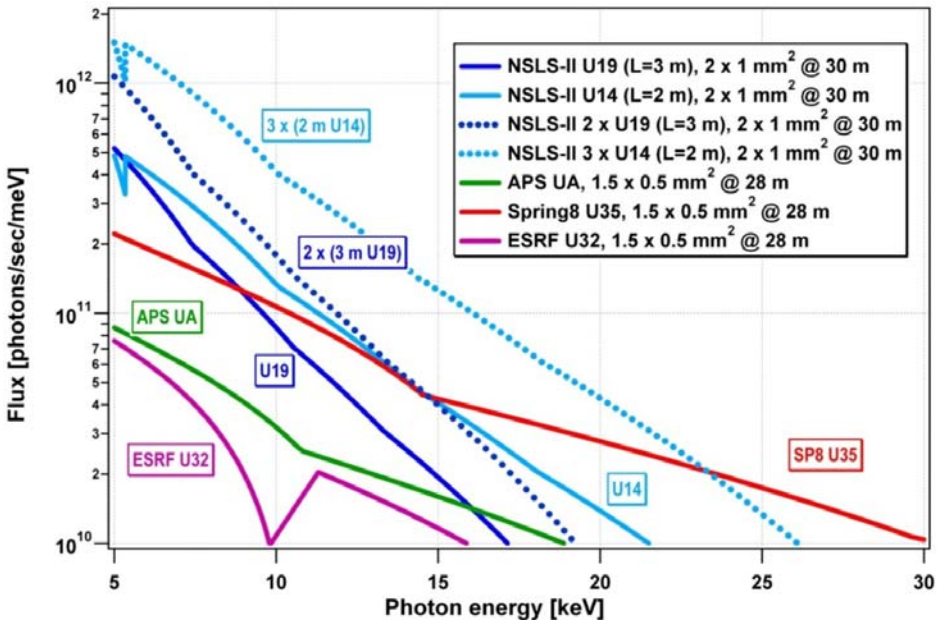

Figure 1.1. Flux comparison of various devices at NSLS-II and elsewhere, as measured in ph/s/meV. The light blue dotted curve shows the increase associated with placing three 2 m-long U14 undulators in a single straight at NSLS-II. The solid blue curve is for one 3 m-long U19 undulator.

Another option being considered is to optimize the undulator parameters to maximize the peak flux at the primary energy of the beamline. Figure 1.2 shows a comparison between a U17 and a U19 undulator of the same length. With a similar strength of the magnetic field, the U17 is expected to deliver a factor of 2 more flux at around 9 keV compared to the U19. Potentially, this type of optimization can be done for each individual beamline. There is therefore some cost implication for the additional design effort. However, the impact on the accelerator systems would be minimal.

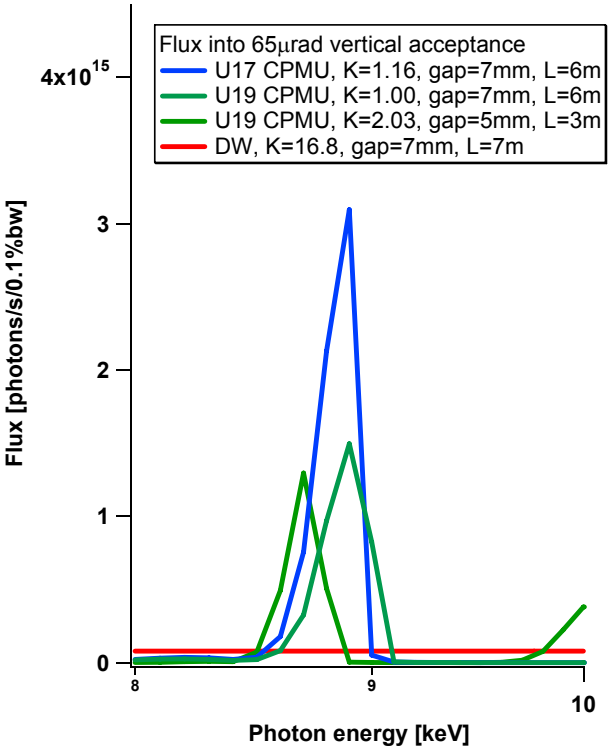

Figure 1.2. Flux comparison of various devices at NSLS-II. Here a U17 with a similar strength of magnetic field is expected to deliver a factor of 2 more flux than a U19 at ~9 keV.

In order to provide the possibility of accommodating two 3m U19 or three 2m U14 undulators, the longer 9.3m high-β straight section of the current storage ring design will be needed. Even for a single U19 undulator, there are other benefits associated with a high-β straight section for the beamline, due to the differences in the beam size and divergence between the low-β and the high-β straight section. As shown in Table 1.2, the horizontal beam size increases by about a factor of 3, whereas the angular divergence decreases by about a factor of 3.5, on moving from a low-β to a high-β straight section. This leads to a corresponding increase of horizontal source size and decrease of horizontal divergence by about a factor of 3 (Table 1.3). Consequently, the horizontal photon beam size reduces by more than a factor of 2 as a result of the reduced beam divergence as it travels downstream of the beamline. The heatload delivered onto the first optics within the central cone of the photon beam reduces also by a factor of 3 (Table 1.4). It should be noted that the flux within the central cone remains essentially the same between the low-β and the high-β straight section. Therefore, the use of a high-β straight section allows a smaller horizontal aperture with no cost to the flux. The heatload on the first optics is reduced to a manageable level, even for two U19 undulators. The smaller horizontal beam size also allows the use of shorter mirrors for the horizontal plane.

Note that a U20 is currently in the baseline device. Calculations show that there are minimal differences between the U19 and U20 in terms of their performance. The discussions in the subsequent sections will still assume the U19 device for convenience.

Table 1.2 Beam parameters assuming eight damping wigglers with 0.55nm-rad horizontal emittance.

Parameters		Low β	High β	Units	Ref.
Emittance	ε_x (horizontal) ε_y (vertical)	0.55 0.008		nm · rad	2,3
Beta function	β_x (horizontal) β_y (vertical)	1.5 0.8	18 3.1	m	3
Energy spread		0.0005 - 0.001		-	3
Beam size (sigma)	σ_x (horizontal) σ_y (vertical)	28.7 2.5	99.5 5.0	μm	Calc.
Angular divergence (sigma)	σ'_x (horizontal) σ'_y (vertical)	19.2 3.2	5.5 1.6	μrad	Calc.

Table 1.3 Source parameters of a U19 operating at several conditions in a low-β and a high-β straight section.

K	N	E, keV	Source size (σ), μm				Angular Divergence (σ), μrad			
			Low-β		High-β		Low-β		High-β	
			H	V	H	V	H	V	H	V
2.03	1	1.47	29.3	6.2	99.7	7.5	22.5	12.3	13.1	12
1.713	5	9.1	28.8	3.4	99.5	5.5	19.8	5.7	7.3	5.0
0.981	3	9.1	28.8	3.4	99.5	5.5	19.8	5.7	7.3	5.0

Table 1.4 Power from a U19 undulator in a low-β and high-β straight section delivered to the first optics at 30 m from the source through an angular aperture defined by 4σ (H) x 4σ (V) of the source divergence.

Distance, m	K (N)	Low-β			High-β		
		Ang. Aperture (HxV), μrad²	Beam Size, (HxV), mm²	Power, W	Ang. Aperture (HxV), μrad²	Beam Size, (HxV), mm²	Power, W
30	1.713 (5)	79.2 x 22.8	2.4 x 0.7	118	29.2 x 20.0	1.0 x 0.6	38
30	0.981 (3)			65			21

1.4 Sector Layout

The Inelastic X-ray Scattering beamline will occupy only the insertion device port of a sector with a long high-β straight section. Nevertheless, the required floor space to accommodate the 1meV endstation may be extended to the floor space of the adjacent beamline on the bending magnet port, which should be given due consideration regarding whether and how the bending magnet port will be used in future.

1.4.1 Front-End Layout

The current generic layout of the front-end for a long, high-β straight section is shown in Figure 1.3. As shown, this front-end layout is compatible with the current design of the IXS beamline. However, the design can be further optimized and coordinated with components planned for the first optical enclosure (FOE) of the beamline, which may provide some cost savings and allow for more efficient use of floor space in the experimental hall. For example, the space between the fast gate valve (FGV) and the second x-ray beam position monitor (XBPM-2) can be used to accommodate the X-Y slit that defines the x-ray beam for the first optical component of the beamline (i.e., the first crystal of the high heatload double crystal monochromator). Other components that should be included in the front-end include (removable) filters and screen monitors at a few locations, for diagnostics during commissioning.

A U19 undulator is expected to generate a total power of 11.2 kW and a peak power density of 77.86 $kW/mrad^2$. If two of this device are used, the total power and the power density will be doubled. The front-end must be designed to handle these power loads.

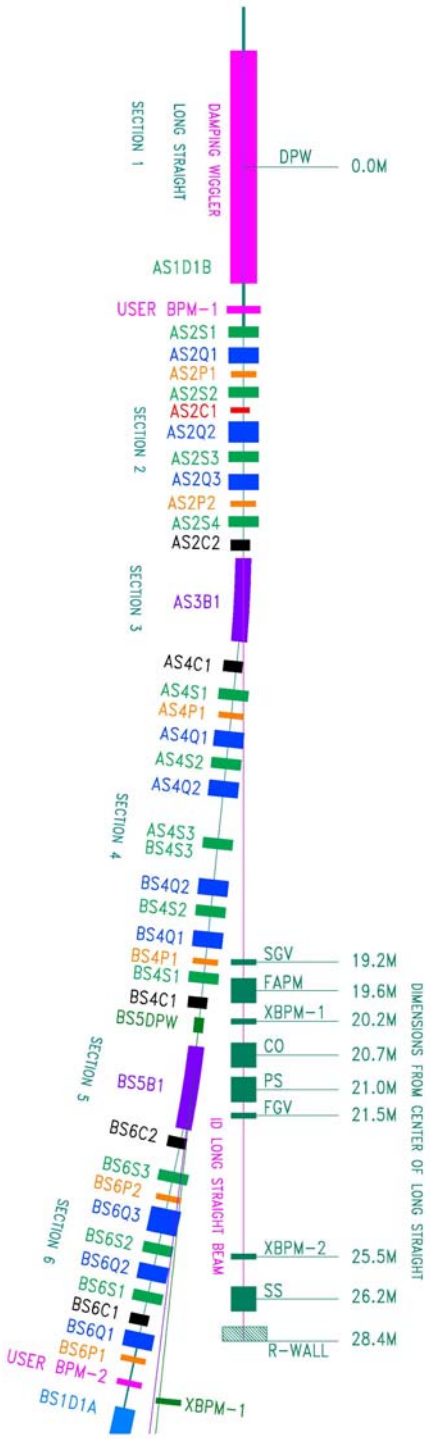

Figure 1.3 Generic layout of the front end for a long, high-β straight section. Components as shown include a slow gate valve (SGV), a fixed aperture mask (FAPM), two x-ray beam position monitors (XBPM), a lead collimator (CO), a photon shutter (PS), a fast gate valve (FGV), and a safety shutter (SS). Positions shown in meters are distance from the center of the straight section.

1.4.2 Beamline Layout

A CAD drawing of the beamline and endstations showing the general layout of the beamline is given in Figure 1.4. Functionally, there are four major optical components before each endstation. These include the high heatload double crystal monochromator (DCM), a vertical collimating/focusing mirror (VCM), a high-resolution monochromator (HRM), and a set of KB focusing mirrors. For the 0.1meV endstation, the HRM will be an inline monochromator based on the CDDW scheme [Ref]. For the 1meV endstation, the optical scheme depends on the approach we will use and will be described in more detail later. All these optical and other beamline components are housed in three enclosures. The first one (the first optical enclosure: FOE) is for the white beam components including the high heatload DCM, and the other two are for each of the two endstations. The VCM is placed in the FOE for convenience. The HRM for each endstation is considered as an integrated part of the endstation, and is therefore housed with the endstation in the same enclosure.

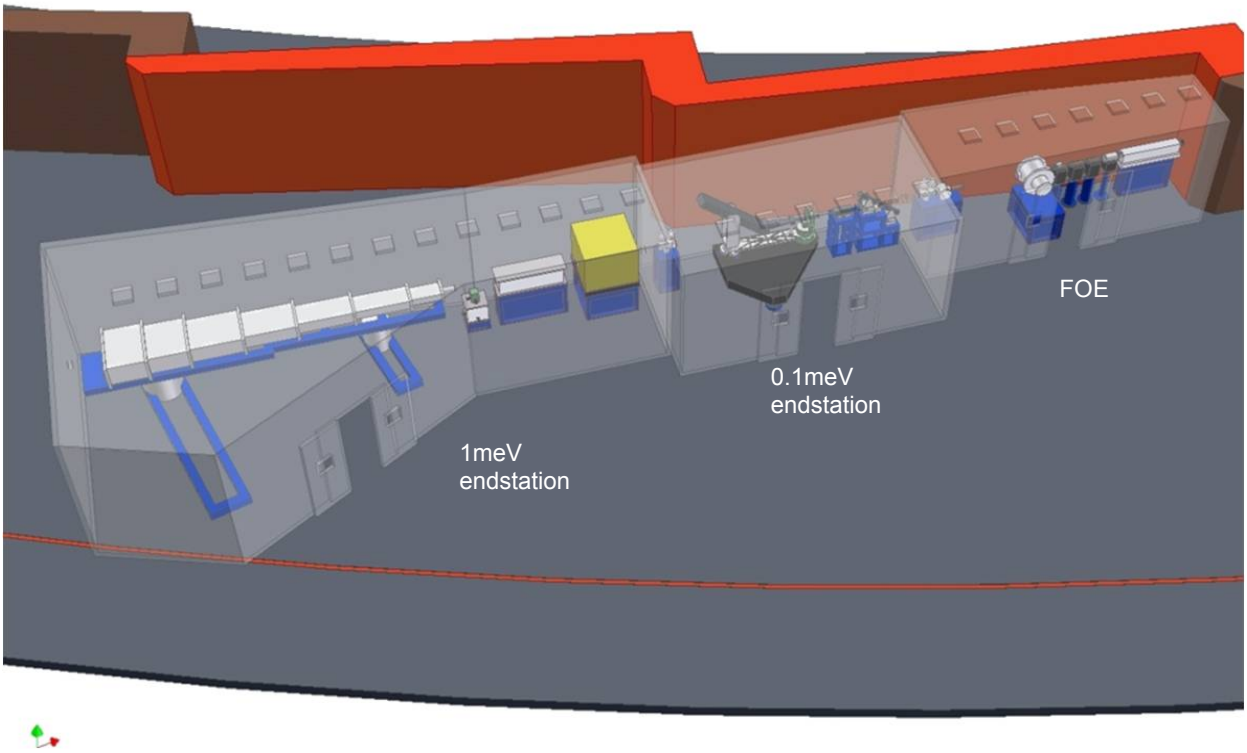

Figure 1.4. Schematic layout of the Inelastic X-ray Scattering (IXS) beamline, showing (right to left) the first optical enclosure (FOE), the 0.1meV endstation, and the 1meV endstation.

1.4.2.1 Survey and Alignment Plans

All beamline components will be surveyed and aligned in place by NSLS-II staff. To facilitate ease of alignment, all components will be fiducialized to external reference points on their table during assembly. All components are designed with a liberal tolerance allowance greater than 0.5 mm. Where necessary, laser trackers will be used which provide alignment precision to ~ 50 microns.

1.4.2.2 Utility Layouts

We will need power panels for single phase 100V and 200V rated to 100Amp each, and 3 phase 200V to 300Amp, distributed to the hutches and control areas. For each hutch, there should be de-ionized and chilled

water, compressed air, N2 and He gas distribution system. For the FOE LN2 outlet is required for the cryogenic cooling system of the DCM. The two experimental hutches will require temperature control to ±0.1 K.)

1.4.2.4 Beamline Vacuum System

The beamline vacuum will be separated from the front-end by a Be window. All beamline components will be designed to ultrahigh vacuum (UHV) standards. The beamline will be operated in most part in high vacuum level. Turbo pumps backed up by oil-free roughing pumps will be used for the pumping stations. High vacuum will be maintained by ion pumps where necessary (for concerns of vibration, for example). A rough vacuum pumping system is planned for each of the endstations for use in pumping sample chambers, flight paths, etc.

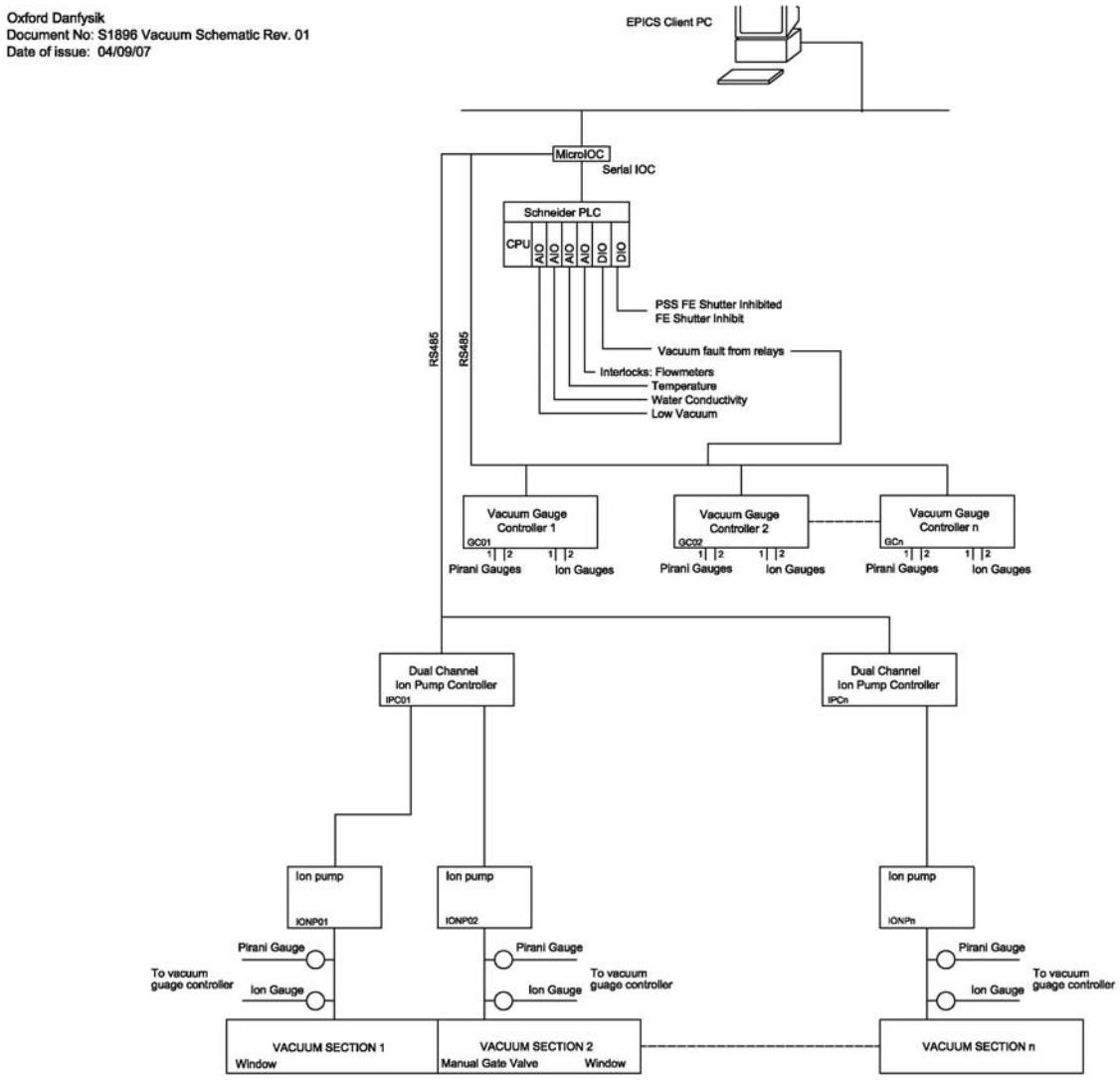

Figure 1.5. Vacuum schematic for the inelastic x-ray scattering beamline.

Figure 1.5 provides a schematic of the vacuum system for the IXS beamline. Vacuum gauge controllers are used to monitoring vacuum level measured by Pirani and ion gauges mounted on different beamline components.

Ion pump controllers provide power to each of the ion pumps used on the beamline. High-voltage splitter units are used, where necessary, to power more than one pump per output channel.

1.4.2.5 Data Acquisition System and Motion Control

The contents of the signal schematics are shown in Table 1.5. The 8-axis motion control boxes having RS232, USB, and Ethernet interfaces are customized to suit the beamline motorized axis. They also have built-in micro IOCs. Separate micro IOCs control the vacuum pump controllers, vacuum gauge controllers, DPT controllers, current amplifiers, and CCD cameras.

The EPS PLC has analog input and digital input and output, and is linked to solenoid valve actuators, fluorescent screen actuators limits, thermocouples, water flow meters, vacuum interlocks, vacuum gauge controllers, cooling water flow meters in the heat exchangers, thermocouples in the heat exchangers, and water conductivity probes.

The PSS shutter is controlled from the PSS and sends and receives status signals to and from the EPS PLC.

The micro IOC controlling the vacuum system uses RS485 protocol for communication with the pump and gauge controllers. Vacuum gauge controllers are integrated with the EPS system to monitor vacuum level in different sections of the beamline.

Piezo actuators and a bimorph mirror will need vacuum interlocks linked to the vacuum gauge controllers. The cryocooler is connected via Ethernet to a dedicated IOC, which is linked to the PSS. The Y-Z profile monitor is connected to a 32-channel electrometer.

Table 1.5. Controls schematics for the IXS beamline.

Beamline Component	No. of units	Number of Elements per Unit											
		Controlled by 8 axis Motion Control units					Controlled by EPS PLC			Controlled by micro IOC			PC
		Stepper/ Pico Motor	Server Motor	Limit/ datum switch	Encoder	Ref point	Flow meter	Thermo-couple	Solenoid valve actuator.	CCD camera	DP control unit	Current amplifier	
Beamline control system	1												1
Fixed mask	1						1	1					
Blade BPM	1	2		4			1					1	
CVD Diamond	1						1	1					
Bremsstrahlung collimator	1						1	1					
White Beam Slit (H **or** V)	2	1		2	1								
Gate Valve	16			2					1				
VFM/VCM	2	5		10	5	5					1		
HFM (bimorph)	1	5		10	5	5							
Bimorph PSU	1												
Beam shutter	3			4				1	1				
Fluorescent screen (water cooled)	1			2			1		1	1			
Fluorescent screen	5			2					1				
DCM	1	5	1	8	7	6	1	3			1		
Cryocooler	1												1
White beam / bremsstrahlung stop	1						1	1					
QBPM	5	1		2								1	
Y-Z profile monitor	1								1				
Monochromatic slits	10	2		4	2	2							

1.4.3 Beamline Components

Table 1.C.1 (see Appendix C) lists the position and size of different beamline components of the current design. Space between the main components will be filled with vacuum bellows and pipes of suitable length. The table also lists different sections of the beamline vacuum system. Positions of the beamline components are specified with respect to the center of the low-β straight section, which was used in the initial stage of the design study. It assumes the distance from the source to the external surface of the shield wall to be at 26.7m, and the distance to the end of the beamline at 66.8m.

The decision to use a high-β straight section will change the shield wall position to 28.6m, and therefore all components listed in Table 1.C.1 will need to be shifted downstream by 1.9m.

Important dimensional constraints for the high-β straight section are as follows:

- Distance from the source to the external surface of the shield wall: 28.6 m
- Maximum source to end of the beamline distance: 60.8 m

Several important considerations have been taken into account in the suggested layout of the main beamline components, which include:

- Share as many common endstation components as possible, to reduce the total cost of the project and complexity of the design.
- Reduce to a minimum the number of optical elements (crystals, mirrors, windows, etc.) put into the beam, to maximize the flux.
- Use most of the available fan of the x-ray beam, to keep the lengths of the optical elements within reasonable limits.
- Create an infrastructure and basis for further R&D that will follow the preliminary design.
- Provide enough flexibility for further beamline design based on the outcome of anticipated extensive R&D.
- For costs to be estimated realistically, include in the early design not just the main components, but all components that are not likely to be affected by further design changes.
- Fit the beamline components into the available floor space and identify any changes to the position of the walls needed to accommodate the equipment.

1.4.3.1 White Beam Slits

The white beam slits, currently planned as part of the FOE components, define the X-ray beam from the undulator source to the first optics of the beamline. If the X-Y slits are to be implemented in the front-end, this white beam slits may no longer be required.

Figure 1.6 shows the position of the white beam slits upstream of the high heatload monochromator. The slits consist of 2 L-shaped absorbers arranged in series along the beam (the downstream one being rotated by 180°) to define the aperture. Each absorber therefore defines two edges of the beam. Each absorber is moved laterally and vertically by external translation stages. There are edge-welded bellows before, between and after the two absorbers, which allow the movement of the slits relative to the beam. The slit mechanism is mounted on a synthetic granite-filled mild steel frame for stability and vibration rejection.

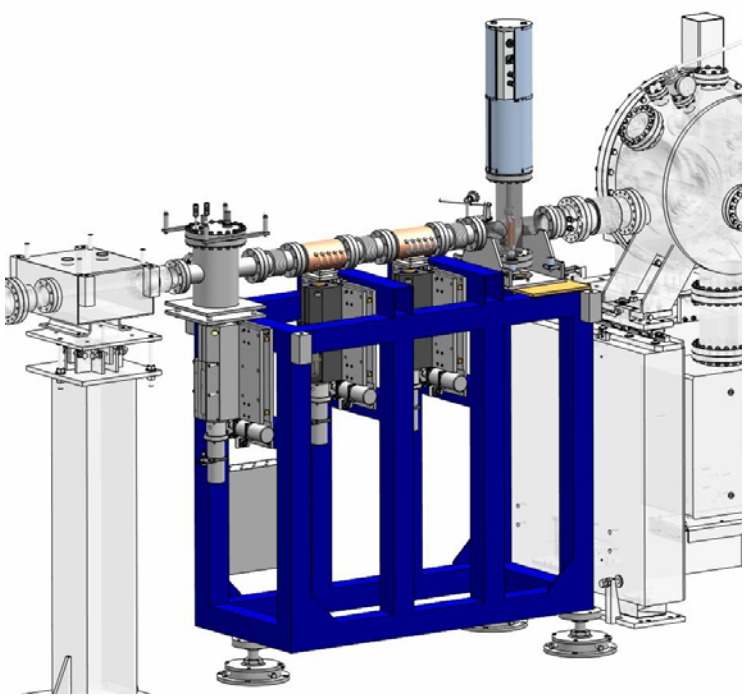

Figure 1.6. White beam slits assembly.

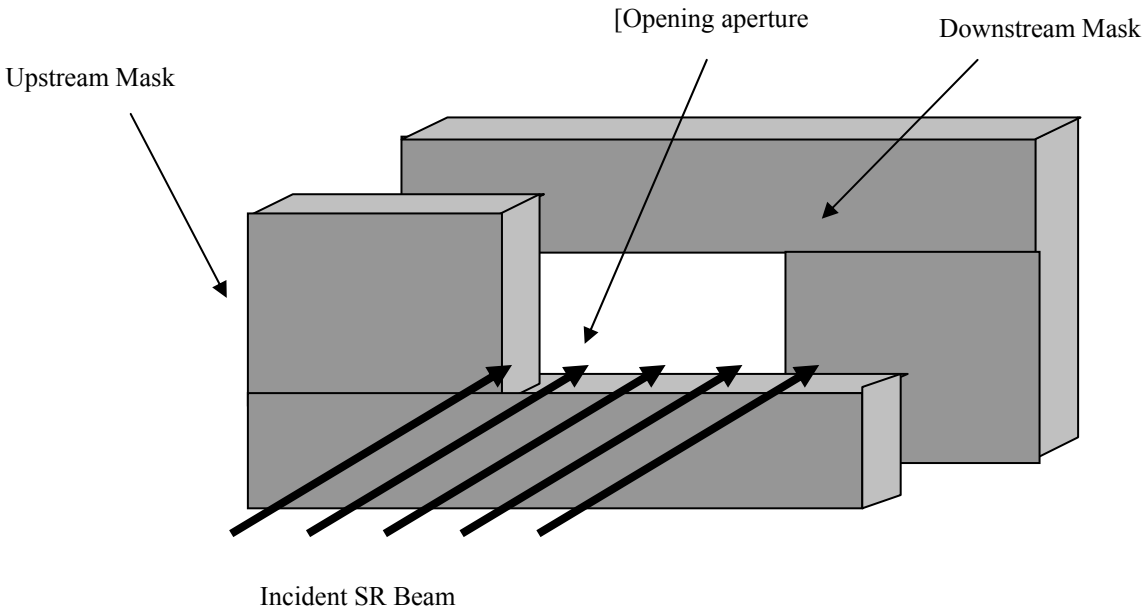

Figure 1.7. White beam slits schematic.

1.4.3.2 Bremsstrahlung Collimator and Beam Stops

The Bremsstrahlung collimators are typically made of 300 mm of lead and their dimensions are calculated from the ray tracing. We will use one of the collimators immediately after the CVD Diamond window/filter.

The Bremsstrahlung collimator is located immediately downstream the fixed mask defining the beam.

A Bremsstrahlung stop is also anticipated after the DCM. Depending on the detailed design it will be made of lead (out of vacuum) or Tungsten (in vacuum).

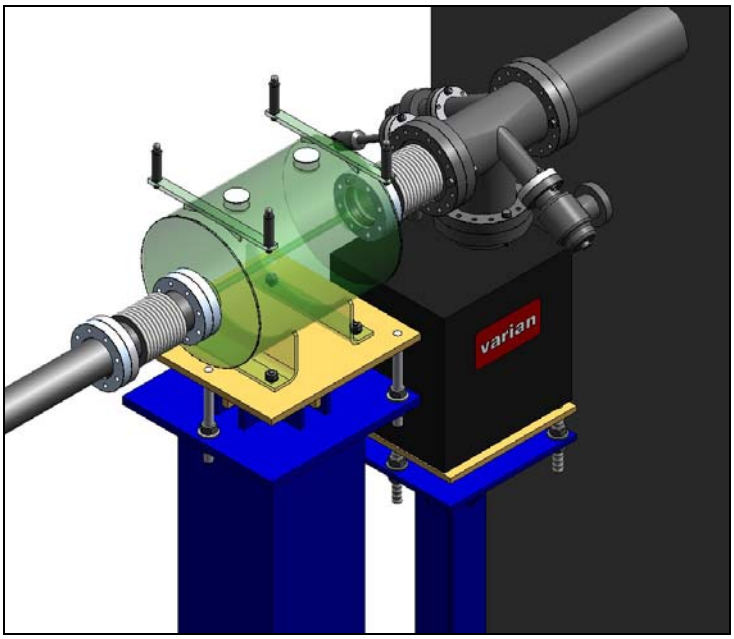

Figure 1.8. Pb collimating assembly.

1.4.3.3 High-Heatload Monochromator

A cryo-cooled Si(111) DCM with no sagittal focusing on the second crystal should provide energy resolution of ~10^{-4}, fixed exit beam height and operate across the requested energy range from 7 keV to 12 keV. Expected performance parameters of the DCM and some useful information are given in Table 1.6. We also assume 25 mm vertical offset between the incoming and outgoing beams and that beam 'walk' alone the second crystal as the energy changes will be taken by longitudinal translation of the crystal.

The results in show that

- The energy resolution is expected to be from $1.77 \cdot 10^{-4}$ to $2.45 \cdot 10^{-4}$.
- The Bragg angles are from 9.5° to 16.4°. The Bragg angle calculation assumes the lattice constant of Si(111) of 5.4309 Å.
- Perpendicular translation of the 2nd crystal over the energy range is about 0.3 mm.
- Longitudinal translation of the 2nd crystal over the energy range is approximately 32 mm.

- The footprint of the beam at the crystals of the Si(111) monochromator at all energies is less than 3.0 mm x 5.5 mm assuming 4σ (H) x 6σ (V) opening of the beam. Vertical size of the beam at the DCM position is about 1.0 mm.
- The lengths of monochromator crystals should be less than 177 mm to avoid shadowing.

The design of the DCM should meet stability requirements and be able to withstand high heat loads as discussed earlier.

It might be possible to use a water cooled DCM but more R&D is needed to prove this is a feasible. We therefore have provided a typical specification for a water cooled monochromator. The BNL water cooled system will most likely use much smaller vertical beam offset, of about 25 mm, than in the example and long second crystal to eliminate longitudinal translation and improve stability. The second crystal will be translated vertically to keep fixed offset of the beam.

The power density could however be very high, particularly when two U19 undulators will be used simultaneously in-line and at the same undulator gap as we have discussed earlier. We therefore believe that most likely a cryogenically cooled system will be needed. We therefore provide an appropriate functional specification for such a system which is being built for ASP SAXS beamline. The DCM is designed to operate at energies of 5-20 keV, has a fixed offset of 25 mm and uses a set of Si(111) crystals. The DCM is designed to achieve angular beam stability of 200 μrad that should be adequate for the current application. As the technology continuously improves using a cryogenically cooled monochromator instead of water cooled one does not create any unnecessary risk for the project.

Modifications to the standard design that should be considered include reducing the beam offset and using long high quality second crystal instead of longitudinal translation to improve stability.

Table 1.6. Performance parameters of the Si(111) DCM.

Parameters	Energy, keV		
	7	**9.1**	12
Wavelength, Å	1.7712	1.3625	1.0332
Bragg angle θ_B, deg	16.4058	12.5482	9.483
Reflectivity (double reflection)	0.85	0.91	0.94
Energy resolution			
Rocking (Darwin) width[1], μrad	39.1586	29.6027	22.2161
Bandpass due to source size	9.2×10^{-7}	1.2×10^{-6}	1.6×10^{-6}
Bandpass due to accepted angular divergence	1.2×10^{-4}	1.5×10^{-4}	2.1×10^{-4}
Resolution of the DCM	1.77×10^{-4}	2.04×10^{-4}	2.45×10^{-4}
Resolving power[2]	5649	4904	4079
Crystal size and position			
Vertical offset between incoming and outgoing beams, *D*, mm		25	
Perpendicular offset between 1st and 2nd crystals[3], mm	13.0	12.8	12.7
Longitudinal offset between the crystals[4], mm	44.3	57.5	75.9
Maximum beam footprint[5]			
transverse to the beam, mm	3.0		
along the beam, mm			6.2
Maximum length of crystals at no beam shadowing[6], mm	177		

Notes: 1) Intrinsic resolution of Si(111) is $\left(\frac{\delta\lambda}{\lambda}\right)_{cryst.}$ = 1.33 · 10^{-4} [30]. The rocking (Darwin) width is $\Omega = \frac{\delta\lambda}{\lambda}\tan\theta_B$.

2) The resolution is determined by the width of the rocking curve of the crystal, beam opening angle and size of the source

$$\frac{\Delta E}{E} = \sqrt{(\Delta\theta^2_{source} + \Delta\theta^2_{slit})\cot^2\theta_B + \left(\frac{\delta\lambda}{\lambda}\right)^2_{cryst.}},$$

$$\Delta\theta_{source} = \sigma_y / p \text{ and } \Delta\theta_{slit} = \min(\sigma_y^{'}, s_v)/p,$$

where σ_y is the vertical source size (FWHM), $\sigma_y^{'}$ is the vertical divergence of the beam (6 σ), s_v is the opening of the monochromator vertical entrance slit and *p* is a distance from the source.

Resolving power of the monochromator is reverse to the total band pass, i.e. it is $\frac{E}{\Delta E}$.

3) The distance, X, measured perpendicular to the optical surfaces of the crystals: $X = \frac{D}{2\sin\theta_B}$, where D is the constant vertical offset between incoming and outgoing beams.

4) The distance, Y, measured along the surface of the crystals: $Y = \frac{D}{2\cos\theta}$, where D is the constant vertical offset between incoming and outgoing beams. The longitudinal offset shows beam walk parallel to the surface of the crystals as the Bragg angle changes. To maintain the constant beam offset, D, the X and Y should satisfy the condition $\frac{1}{X^2} + \frac{1}{Y^2} = \frac{4}{D^2}$.

5) The beam footprint depends on the rms size and divergence of the incoming beam, DCM distance from the source and the Bragg angle so that

$$F = \sqrt{\sigma^2_{x,y} + (\sigma^{'}_{x,y}\cdot p)^2};\ F_x = F;\ F_y = F/\sin\theta,$$

where $\sigma_{x,y}$ and $\sigma^{'}_{x,y}$ are the size and divergence of the source, correspondingly, p is the distance from the source and θ is the Bragg angle.

6) To avoid shadowing of the beam at high Bragg angles, the lengths of the crystals should match the vertical beam offset.

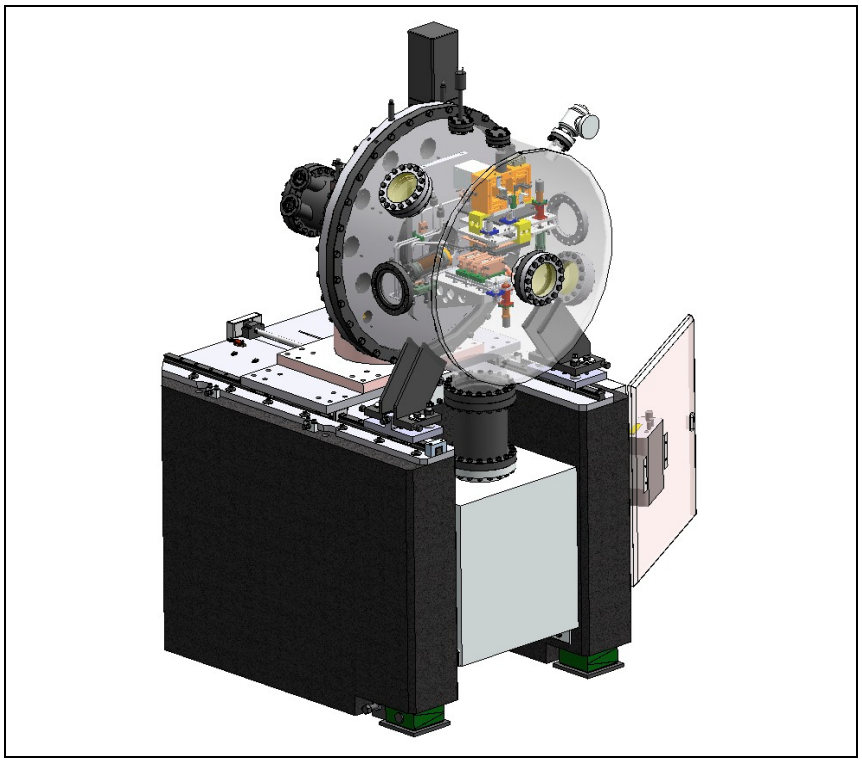

Figure 1.9. Isometric view of the Si(111) DCM.

1.4.3.4 White Beam Shutter

Special requirement for the beam shutters and their integration with the Personnel Protection System will be discussed with the vendor before the detailed design starts.

1.4.3.5 Collimating and Focusing Mirrors

As it has been discussed earlier, the beam line is expected to have few mirrors for collimating and focusing the beam in horizontal and vertical planes. Preliminary analysis shows that full energy range of 7 -12 keV can be covered without changing the angle of incidence while providing good transmission of the x-ray beam over the whole range.

Increase of the angle of incidence is favorable for reducing the cut-off energy, lengths of the mirrors and improving harmonic rejection, but the reflectivity of the mirrors decreases. We have considered using bare Si, Silica (SiO_2, less expensive option and good alternative to Si for using with monochromatic beams) and Pt, Pd and Rh coatings and concluded that Rh and bare Si or Silica are most suitable for the energy range. Pd is very similar to Rh but the latter has slightly better reflectivity. Reflectivity of Pt shows few absorption edges and it is more suitable for higher energies.

Most mirror suppliers will guarantee densities of Rh in the coatings to be better than 90% of the bulk material which is 12.41 g/cm^3 [28]. We therefore assume in this analysis the density of Rh of 11.17 g/cm^3 for calculating reflectivity of the mirror stripes. The densities are usually lower, about 85% of the bulk, for bimorph mirrors. The lower density means slightly lower reflectivity and lower cut-off energies at similar angles of incidence. The data in Figure 1.10 show that replacing Silica with Silicon as a mirror substrate increases the cut-off energy by approximately 300 eV. As the density of Rhodium decreases from 90% to 85%, the cut-off energy decreases by about 550 eV.

The density of Si, 2.33 g/cm^3 [28], is slightly higher than the density of Silica, 2.2 g/cm^3 [29]. Usually Silica is used as a substrate for making mirrors to focus monochromatic beam and silicon is used to make mirrors operating in a white beam.

Figure 1.10 shows variation of the critical angle of the mirrors versus energy for Si, Silica, Rh (and Pt). The critical angles were calculated as $\alpha_c = \sqrt{2\delta}$, where δ is a real part of the refractive index of material. Incidence angle of the mirrors should ensure that the low energy beam is not contaminated by the beam of higher energy. Also it is not desirable to make mirrors much longer than 1 m. But the reflectivity of the mirrors decreases as the angle of incidence increases. Therefore the incidence angle should be optimized taking into account these factors and ease of use.

Useful energy range is defined from 7 keV to 12 keV [2] and from the point of view of ease of use changing the mirror stripe in this region should be avoided. In that case the mirrors could be set at an incidence angle of approximately 4.5 mrad to achieve about 87-89.5% reflectivity using Rh stripe. Higher reflectivity can be obtained using Si or Silica stripe. Reflectivity of Silica, for example, at 3 mrad incidence at 7 – 9.5 keV is about 95 - 96.5%. But to cover the whole energy range of 7 – 12 keV the incidence angle should be much smaller, 2.5 mrad.

We therefore suggest operating in one of the three regimes:

- Use Rh stripe and incidence angle of 4.5 mrad.
- Use Rh stripe and incidence angle of 4.5 mrad at energies from 9.5 to 12 keV and Silica stripe and incidence angle of 3.0 mrad at energies from 7 to 9.5 keV.
- Use Use Rh stripe and incidence angle of 4.5 mrad for HCM and HFM and Silica stripe and incidence angle of 3.0 mrad for VCM and VFM.

The last option is probably a good compromise between reflectivity and ease of use. Figure 1.11 shows calculated reflectivity of bare Silica and Rh stripes.

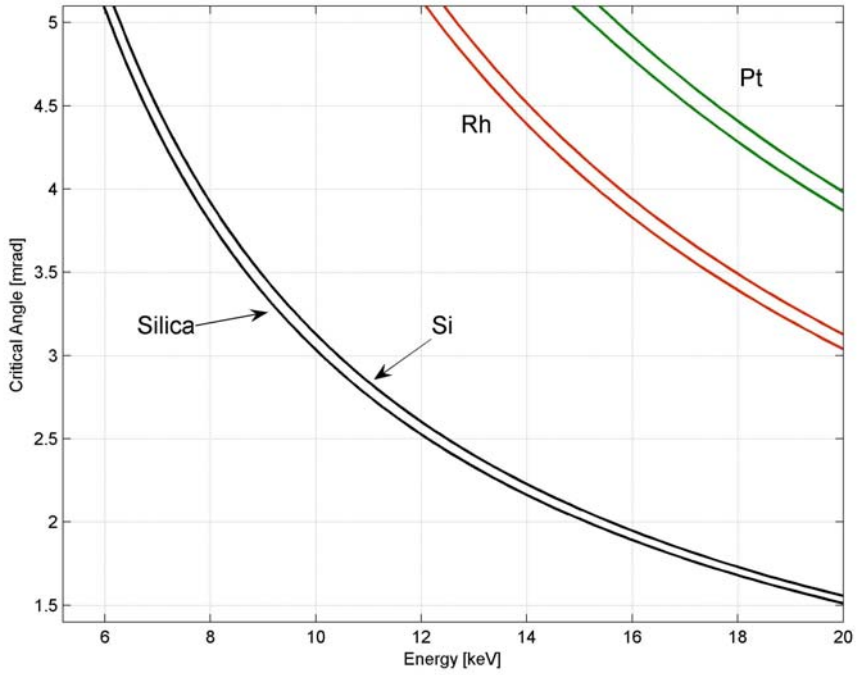

Figure 1.10 Variation of the critical thickness versus energy for bare Silica, Silicon, Rhodium and Platinum. The double lines for Rh and Pt correspond to different densities of the materials: 85% density of the bulk for the lower line and 90% for the upper line.

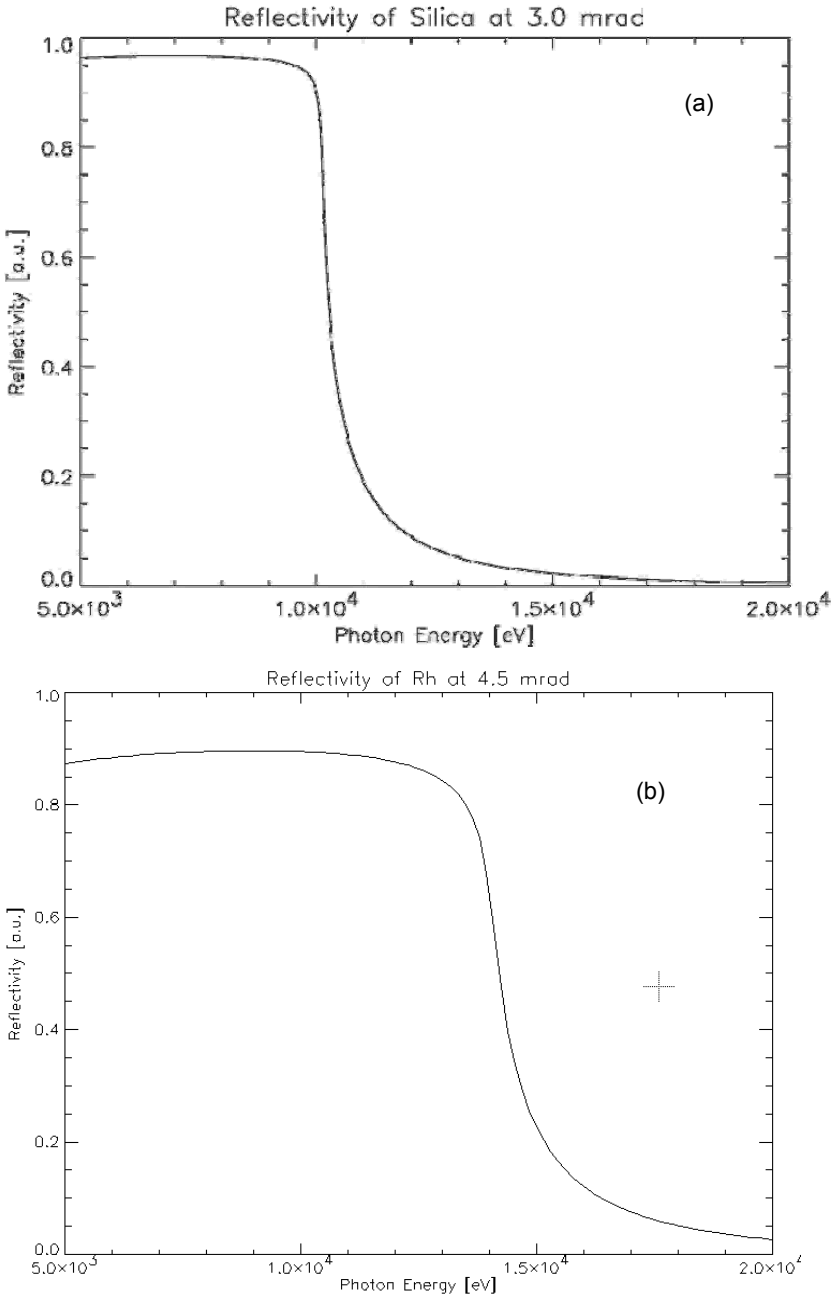

Figure 1.11 Reflectivity of Silica at 3.0 mrad (a) and Rhodium at 4.5 mrad (b)

We assume the HFM and VFM will be bent to a cylindrical shape. The lengths of the mirrors can then be calculated using the expressions given by Peatman [19]:

$$L = P\sin\left(\frac{\alpha}{2}\right)\left(\frac{1}{\sin(\theta_i + \frac{\alpha}{2})} + \frac{1}{\sin(\theta_i - \frac{\alpha}{2})}\right)$$

$$L \approx \frac{2P\sin\left(\frac{\alpha}{2}\right)}{\sin\theta_i}$$

where L is the length of the footprint of the beam on a mirror, P is a source-to-mirror distance, α is the vertical divergence of the beam and θ_i is the grazing angle of incidence of the mirror.

Estimated radii of the mirrors and some other useful characteristics are shown in Table 1.7 for the worse case in terms of beam angular divergence which is at low beta straight and ε_x =0.9 nm-rad. The VCM should have angular acceptance of 10 mrad (H) x 5 mrad (V). We have therefore increased the incidence angle to 5 mrad for that mirror to reduce its length. The cut-off energy of Rhodium at this angle will be 12.6 keV and reflectivity up to 88%. The length of the mirror depends on the amount of space required for the sample area. More accurate values of the parameters will be given after completing ray tracing analysis.

The lengths of the mirrors, particularly of the HCM and HFM ones, will decrease dramatically if the source parameters change. At ε_x =0.55 nm-rad in low beta straight the length will be 670 mm and in a high beta straight it will further decrease to 288 mm at ε_x =0.9 nm-rad and to 247 mm at ε_x =0.55 nm-rad.

Table 1.7 Parameters of the mirrors. Incident beam has angular divergence of 100 μrad (H) x 22.8 μrad (V). The *p* and *q* are source-to-mirror and mirror-to-image distances.

Mirror	Optical distance from source, m	Inci-dence angle, mrad	Coating	Beam Footprint, mm		Bent radius, m	*P*, m	*Q*, m
				Horizontal	Vertical			
VCM	31.88	2.5	Silica	3.2	291	25220	31.88	∞
VFM	39.15	2.5	Silica	3.8	291	336	- ∞	0.42
VCM[1]	40.33	5	Rh	7.6	1014	338	0.76	∞
VFM	74.46	2.5	Silica	3.8	291	516	- ∞	0.645
HFM	38.05	4.5	Rh	846	0.9	650	38.05	1.52
HCM	38.05	4.5	Rh	846	0.9	16911	38.05	∞
HFM	73.36	4.5	Rh	846	0.9	776	- ∞	1.745

Notes: 1) Footprint of the beam at VCM corresponds to angular acceptance of 10 mrad (H) and 5 mrad (V). To increase angular acceptance the VCM has Rh coating and higher angle of incidence.

The KB mirror system will include a bimorph horizontally focusing mirror and a conventional vertically focusing mirror equipped with a cylindrical bender. The bimorph mirror allows changing focus between the sample positions at the first and second endstations and reduces slope errors.

One vertically collimating (VCM) and one vertically focusing mirror will be used in monochromatic beam only. The VCM mirror systems will have capability of removing the optics from the beam delivered to the second, low-resolution, endstation using a backscattering monochromator.

The quality of the optical surface that can be achieved is being continuously improved by mirror manufacturers. We expect this trend will make it possible to purchase much better mirrors in few years time compared to those currently available on the market.

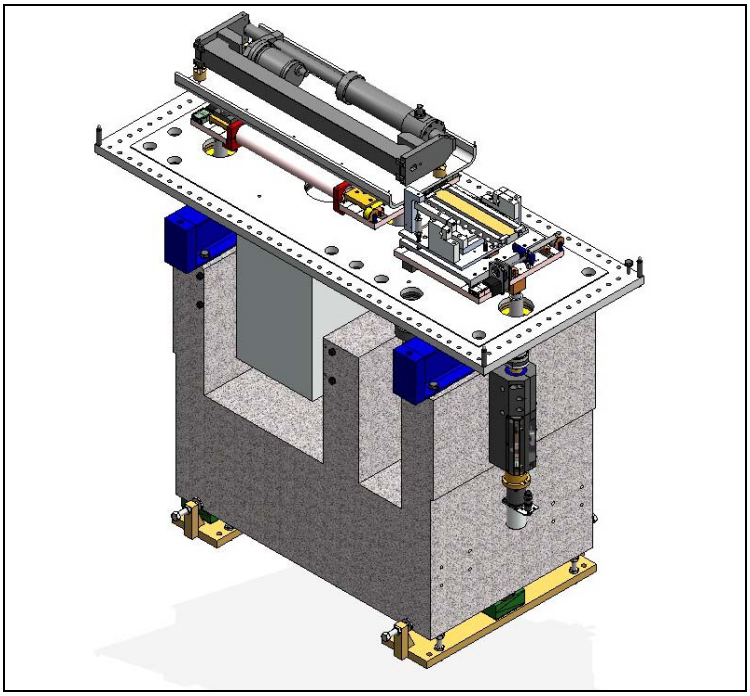

Figure 1.10. KB mirror assembly.

1.4.3.6 Monochromatic Shutter

Special requirement for the beam shutters and their integration with the Personnel Protection System will be discussed with the vendor before the detailed design starts.

1.4.3.7 Vacuum windows

Table 1.6 SiN 200nm window.

Supplier	SPI supplies
Outside frame dimensions	7.5mm x 7.5mm
Window size	1.5 mm x 1.5 mm
Membrane thickness	200 nm
Frame thickness	200 µm
Quantity	Pack of 50

1.4.4 Instruments

1.4.4.1 Endstation 1

End station 1 will have energy resolution of 0.1 meV at 9.1 keV [1]. The resolution will be achieved using novel design of high-resolution monochromator and analyzer optics exploiting an effect of angular dispersion in asymmetric Bragg diffraction predicted by dynamic theory of x-ray diffraction.

Design of the monochromator and analyzer is still subject to a debate. Significant design work and testing is required before the final working configuration becomes available. As it stays now a monochromator using this scheme consists of few Silicon crystals: a collimator, one or two dispersing elements and a wavelength selector. An inline configuration of the monochromator is preferable and the collimator and the wavelength selector could be just different sides of the same crystal, see Figure 11.5.4 in section 11.5.2.3.2 of reference [1]. To achieve a 0.1 meV energy band pass a very large asymmetry angle, of about 89.5^{o}, is required for the dispersing crystals.

The monochromator and the analyser will have an angular acceptance of 0.2-0.3 mrad in the horizontal scattering plane and 0.1 mrad in the vertical plane.

The spot size on the sample should not exceed 20-30 μm (H) x 10 μm (V). This requires a (micro) focused beam on the sample that can be achieved using a standard focusing system. The mirror to sample distance is likely to be of about 100 mm. The minimum distance is to provide some space for the sample environment.
An angular dispersive analyser similar to the monochromator will reflect the beam back to the detector. The backscattering analyser is chosen to reduce the total length of the beam line. An acceptance angle of Y^2 with Y~ 5 to 10 mrad is required. Therefore some collimating optics is needed in front of the analyser. As the asymmetry angle is large an angular acceptance of 2 to 3 mrad in the vertical plane translates into about 2 m long dispersive element length [1].

There will be a Kirkpatrick-Baez (KB) mirror system [2] with graded multilayer mirrors. This is preferred to a parabolic, or curved graded multilayer mirrors or tapered glass capillaries discussed in section 11.5.2.3 of reference [1]. The mirrors will be put after the sample but before the analyser. X-rays leaving the mirror system should match the angular acceptance of the analyser given above. Also the vertical beam size should not exceed 0.5 to 1.0 mm to restrict the length of the analyser crystals.

The spectrometer will be utilising 9.1 keV x-rays and providing an energy resolution of 0.1 meV and a momentum transfer resolution of about 0.1 – 0.4 nm^{-1}.
The energy of the photons selected by the spectrometer will be tuned by varying the temperature of the crystals. Temperature of individual segments of the segmented analyser (consisting of 8 to 10 segments 20-25 cm long) should be homogeneous to 0.5 mK corresponding to 0.01 meV energy shift [1].

1.4.4.2 Endstation 2

The vendor has considered several options for separating the beam used by the endstations. As there is significant uncertainty in the specification of the low-resolution endstation, they started by summarizing designs of the existing beamlines built at ESRF (ID28, ID16) [10,11], SPring-8 (BL35XU, BL11XU) [12-14], and ASP (3 IDC-C, IXS-CDT) [15,16] facilities. In every case there are some collimating optics in front of a high-resolution monochromator (HRM), particularly in a vertical plane. A logical conclusion is that, irrespective of the chosen monochromating scheme based on one of the known configurations of achieving high (meV) energy resolution [17-20], there will be some need for collimating the beam passing after the high

heat load monochromator and before a HRM. Therefore, we can try to use most of the optics from Endstation I at the Endstation II. That should be cost effective and allow saving some space at the second endstation.

It would be ideal to separate the beam going to Endstation II after the DCM, VCM, and HRM of Endstation I. It is unlikely, however, that the HFM can also be used as a HCM for the second endstation, as it needs to be curved to a certain radius during manufacturing. Hence the options are:

1. Design a HRM that will be flexible enough for using at both endstations. This is a risky approach, as it is unclear at present how the monochromator for Endstation II should look and if it is feasible to combine both monochromators into a single unit. To be on a safe side and keep all options open, we should assume that a completely different HRM will be designed for Endstation II. We can safely assume, however, that the HRM at Endstation I could be made capable of passing the beam straight through.
2. The HFM vessel could be used to accommodate a second mirror, the HCM, for collimating the beam at Endstation II. This option looks attractive, but some information on the design of the prospective sample area at Endstation II is needed to ensure there are no serious restrictions for pursuing this approach. It will be necessary to make specially designed gate valves with built-in windows to separate vacuum sections of the beamline so the beam is not attenuated by numerous vacuum windows before reaching the second endstation.
3. Insert a HCM for Endstation II after the high-heatload monochromator. An advantage is that a shorter HCM is needed, but it is difficult to find extra ~1.5 m space within the constraints on the position of the hatch walls. If the HCM is used for Endstation I, the HFM should have a similar length. The disadvantage of using an intermediate mirror is that about 10% of flux will be lost due to reflectivity and slope errors.
4. One option is to offset the beam horizontally using two silicon crystals, but this possibility was eliminated because of spare restrictions.
5. Offset the beam vertically using an additional vertical mirror.
6. Replace a CVD diamond window/filter with a Laue monochromator to create large angular offset between the beam paths to the endstations.

Whichever option, 2, 3 or 5, is selected, provision should be made to allow the second beam to reach Endstation II. The further upstream the mirror is, the more difficult it is to separate the beams. It might be necessary to provide translations or larger apertures to different components until the beams become sufficiently well separated. The vendor suggests implementing option 2 by putting two mirrors facing each other into a single vessel. In that case, the beam path to the second endstation becomes separated by distance x incidence angle x 4 horizontally at the HFM position and by distance x incidence angle x 2 vertically at the VFM position.

To provide enough flexibility for future developments the beamline components should be suitable for operating at energies of 7 – 12 keV. For this energy range, the most suitable mirror coating is probably Rhodium and an optimum incidence angle for the mirrors is 4.5 mrad. At low energies silicon is preferable, but a smaller (about 2.5 mrad) incidence angle is required to cover the entire energy range, and at 2.5 mrad the mirrors become too long; a good compromise is to operate at 3.0 – 3.1 mrad incidence. We would recommend using a bare silicon stripe at energies below approximately 9.0 – 9.5 keV to get about 5% higher reflectivity. As an option, the silicon stripe can be used for shorter, VCM and VFM mirrors. The diagonal offset of the beam at 4.5 mrad (assuming a Rh-coated mirror) will be approximately 20 mm per 1 m distance.

We do not know yet which configuration will be chosen for Endstation II. The options being considered include new asymmetric optics similar to Endstation I or a conventional single-bounce backscattering monochromator and a backscattering analyzer utilizing sapphire or quartz. The disadvantage of the former (or the one suggested by Baron [19]) is due to flux losses at crystals used simultaneously in Bragg reflection and transmission. The latter option appears to offer more diversity for the beamline, and there is a good chance that sufficient progress will be made over the next few years in growing high quality crystals of quartz and/or

sapphire. It sounds reasonable to use scattering in the horizontal plane as suggested in reference [1]. A proposed layout for Endstation II is listed in Table 1.C.1, but it must be noted that the layout may be subject to a major revision if the endstation is to be built on different principles.

Therefore the design of Endstation II may be similar to the recently built beamline BL35XU [13]. The points for consideration and approval include the following:

- Possible use of a pair of Si(111) crystals to shift the backscattered beam vertically by a convenient amount to separate the scattered and incident beams which are otherwise nearly parallel due to backscattering at an angle close to 90^o
- Possible need for vertical scattering analyzer
- More floor space is desirable

1.5 Additional Requirements Imposed on the Conventional Facilities

Temperature Stability

Stability requirements are determined by temperature stability and vibration (natural and self-inflicting), and were extensively discussed at the recent NSLS-II Stability Workshop in April 2007.

The beam stability requirements for different components are based on achieving less than 10% variation of the beam size. According to Shvyd'ko [22], 0.1 meV energy resolution requires <1K temperature stability inside the station. To keep broadening of the reflected beam lower than 10%, temperature variations along the dispersing elements should be within 2 mK [22].

Typical temperature variations measured at ESRF are about 0.5^o [24]. Therefore, 1K temperature stability can be achieved. For demanding beamlines, new high-flow air conditioning units (air renewal rate 20 cycles/hour) are used. Vibrations from air flow are reduced using porous ducts [23]. At the ID22 beamline at ESRF, temperature variations are $< 0.1^o$ over 24 hours [24].

Construction/conventional design measures that reduce thermal effects include choosing low-expansion materials, cooling local heat sources, thermally insulating vessels, moving all control electronics outside the hutches [24], using thermally insulated sand-filled stands, and striving for high thermal inertia [24].

1.6 Additional Requirements Imposed on the Accelerator Systems

Beam Stability

As stated above, stability requirements are determined by temperature stability and vibration (natural and self-inflicting). In terms of beam stability, the requirements for different components are based on achieving less than 10% variation of the beam size.

In addition to the temperature control measures discussed above, Shvyd'ko reports [22] that 0.1 meV energy resolution requires 0.25 μrad incident beam direction stability in the vertical plane and 0.25 μrad relative angular stability of the monochromator and analyzer single-crystal components. A similar requirement for beam stability better than 0.01 meV that would require stability of the incident beam direction (beam angle) better than 0.250 μrad is given in report [23] and its most recent updates [2]. Horizontal angle stability should be 10% of the opening angle. Horizontal and vertical position stability should be 10% of the beam size. It has been pointed out that angular vibration drifts are much worse than linear [24]. This is particularly true for long beamlines like IXS.

References [to be completed]

1-A Appendix A: Ray Tracing Using XOP and Shadow

The vendor conducted ray tracing of the beamline at 9.1 keV using the XOP and Shadow packages to analyze a combined effect of surface distortion of the first crystal of the DCM on beam size and flux at the first sample position. The assumed positions of the optical elements, DCM, VCM, HFM, and VFM, are as given in Table 1.C.1 (Appendix C). The results of the FEA analyses for several of the most important cases are given in Table 1.A.1 below and in Figures 1.A.1 and 1.A.2. Cases 2 and 4 are highlighted in the table, as the beamline is most likely to be used in a high-beta regime.

Table 1.A.1 Results of ray tracing analysis at different heat loads at first crystal of the high-heatload monochromator at 9.1 keV.

Case No.	Model (1xU19, 2xU19)	Spot size at no crystal distortion, μm	Flux at no crystal distortion, ph/s	Spot size, μm	Flux, ph/s
1	Low beta, 0.55 nm-rad, K=0.981, 1xU19, Power = 22 W	2.0 x 1.8	1.50×10^{13}	2.1 x 2.1	1.49×10^{13}
2	High beta, 0.55 nm-rad, K=0.981, 1xU19, Power= 7 W	7.0 x 1.8	1.49×10^{13}	7.0 x 2.0	1.49×10^{13}
2a	As above, but water cooled Si crystal	7.0 x 1.8	1.49×10^{13}	16 x 7.4	1.51×10^{13}
3	Low beta, 0.55 nm-rad, K=1.714, 1xU19, Power = 71 W	2.0 x 1.9	2.88×10^{13}	2.3 x 4.2	2.81×10^{13}
3a	As case 3, but base temperature is 105K to get the hot spot of the crystal at 125 K			2.1 x 0.5	2.92×10^{13}
3b	As case 3, but 2xU19, 115 W	2.0 x 2.0	5.80×10^{13}	2.9 x 5.9	5.14×10^{13}
4	High beta, 0.55 nm-rad, K=1.714, 1xU19, Power = 22 W	7.1 x 1.9	2.81×10^{13}	7.0 x 3.4	2.79×10^{13}
5	Low beta, 0.9 nm-rad, K=1.714, 2xU19, 148 W.	2.6 x 2.0	5.82×10^{13}	3.3 x 5.7	4.68×10^{13}

Corresponding heat loads are given in Table 3.4. Flux at the sample position was calculated over a 20 μm x 20 μm aperture. Mirrors were assumed to be elliptically bent, to show better spot size. The number of rays was converted into flux using the expression

$$\text{Flux[ph/s]} = \frac{\text{N}_\text{T}}{\text{N}_\text{i}} \frac{\Delta E\ [eV]}{E\ [\text{keV}]} I_0\ [\text{ph/s}],$$

where NT is the number of rays transmitted through the optical system, Ni is the number of incoming rays corresponding to the incident flux I0, $\Delta E=3eV$ is the bandwidth over which the ray tracing was performed, and E is the energy of photons in the middle of the bandwidth. The incident flux was calculated using the XUS program from the XOP package.

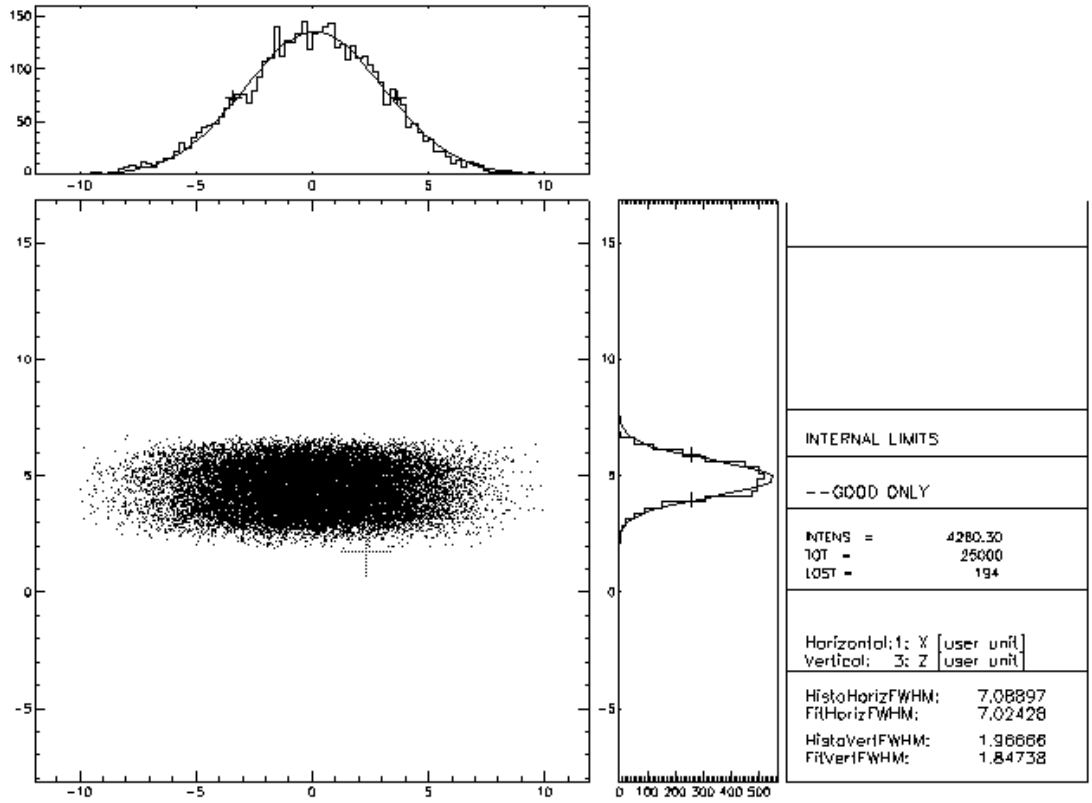

Figure B1. Beam spot at the sample for Case 2 in Table B1. Surface errors due to heating and cooling of the DCM crystal were included in the calculations.

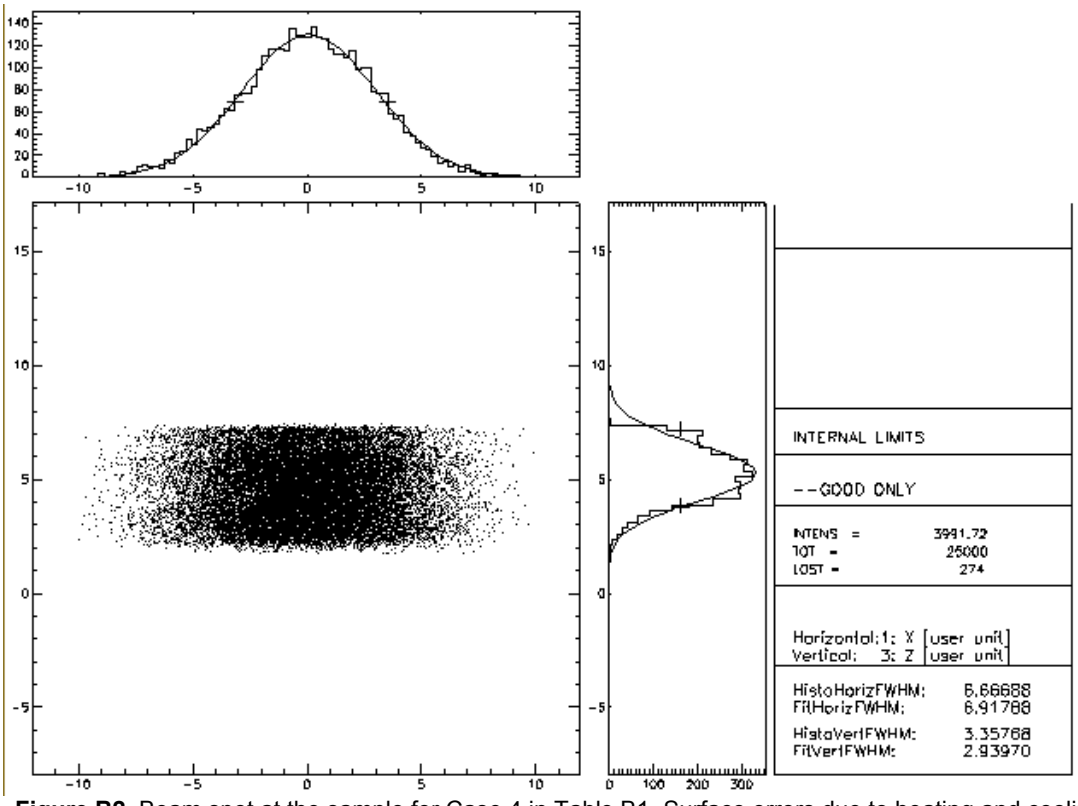

Figure B2. Beam spot at the sample for Case 4 in Table B1. Surface errors due to heating and cooling of the DCM crystal were included in the calculation.

Figure B3 shows a simulation for the same heat load as in Case 2 but for a water-cooled Si crystal. The data show significant broadening of the beam. There would be noticeable loss of flux if it were calculated over a smaller aperture than the 20 μm x 20 μm chosen here.

Results show that in the high-beta regime, the spot at the sample is sufficiently small and of a regular shape even at K=1.714 (Case 4), whereas the flux is nearly doubled compared to the case of K=0.981 (Case 2). The expected resolution of the beamline without the high-resolution optics is shown in Figure B4.

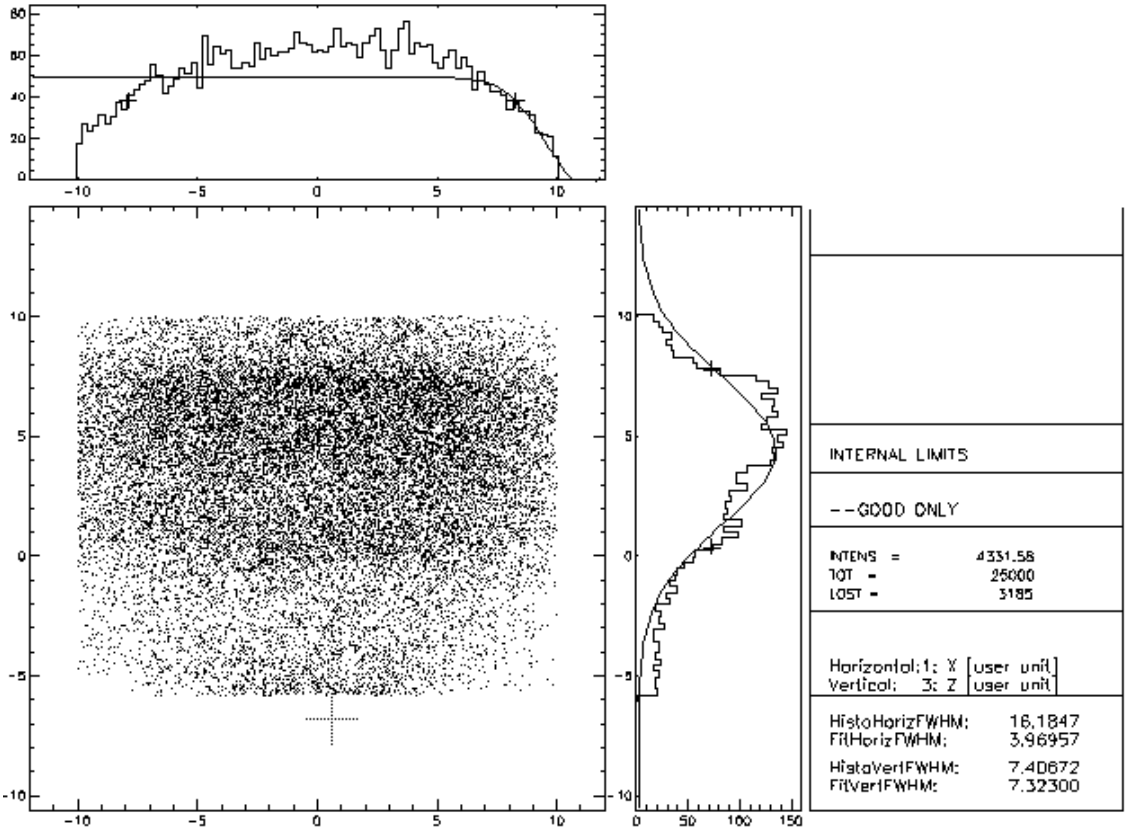

Figure B3. Beam spot at the sample for Case 2a in Table B1. Surface errors due to heating and cooling of the DCM crystal are included in the calculations. The crystal was water cooled.

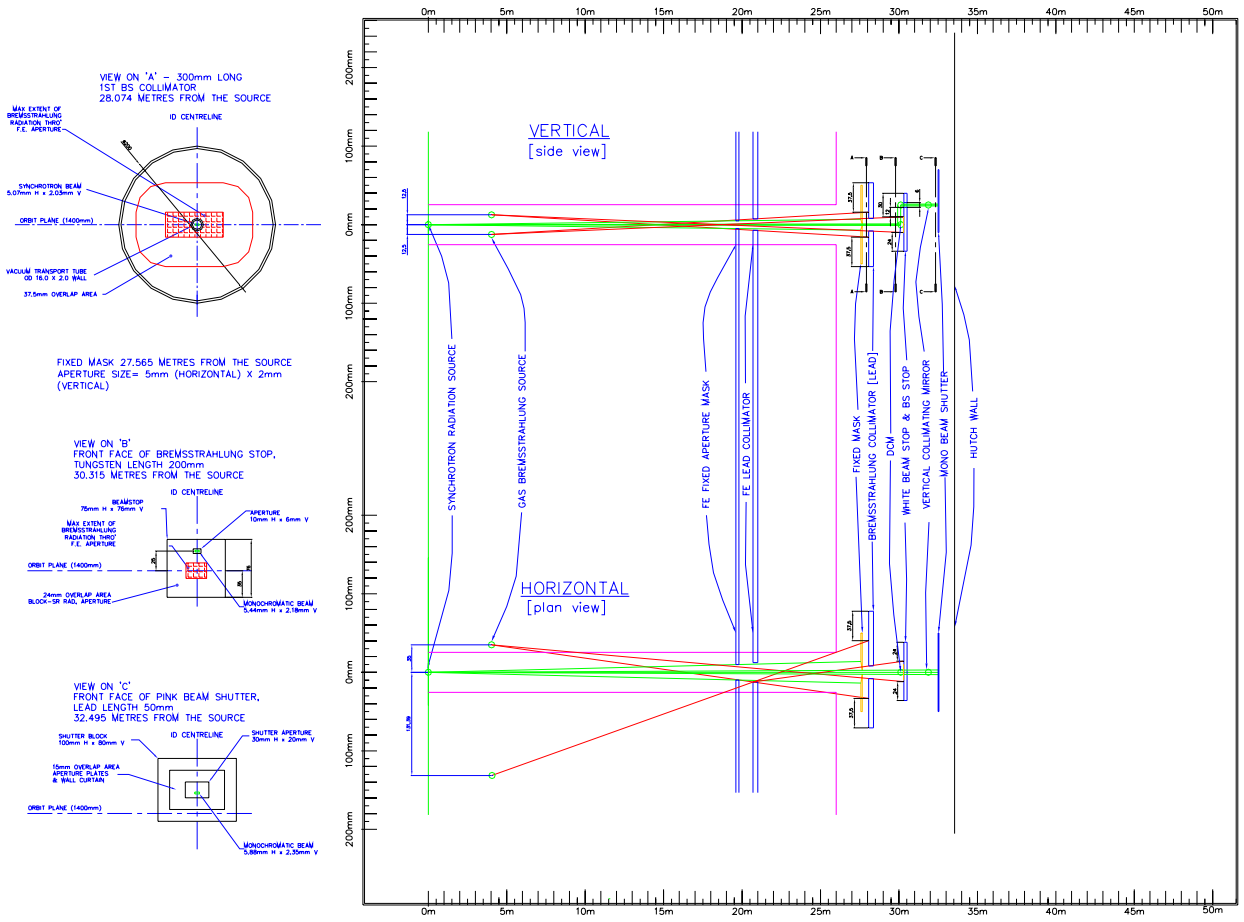

Figure B.4 Bremsstrahlung ray trace diagram for the inelastic x-ray scattering beamline.

1-B Appendix B: Beamline Layout Drawings

This is a possible layout of the IXS beamline showing a two-endstation and back-scattering monochromator configuration.

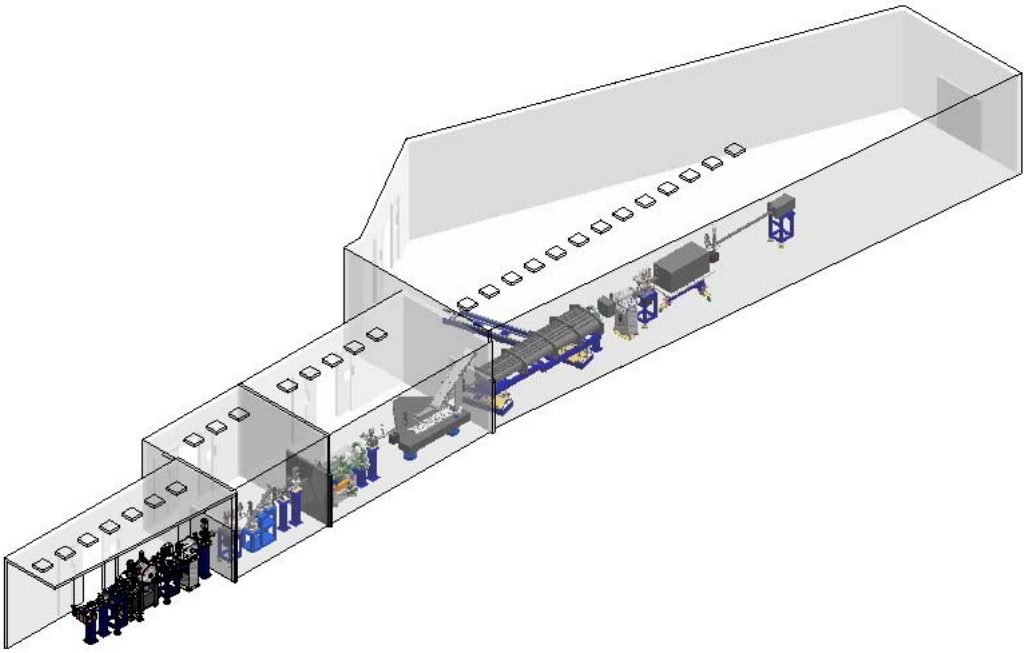

Figure B1. General view of the NSRS-2 IXS beamline and two endstations (Backscattering HRM).

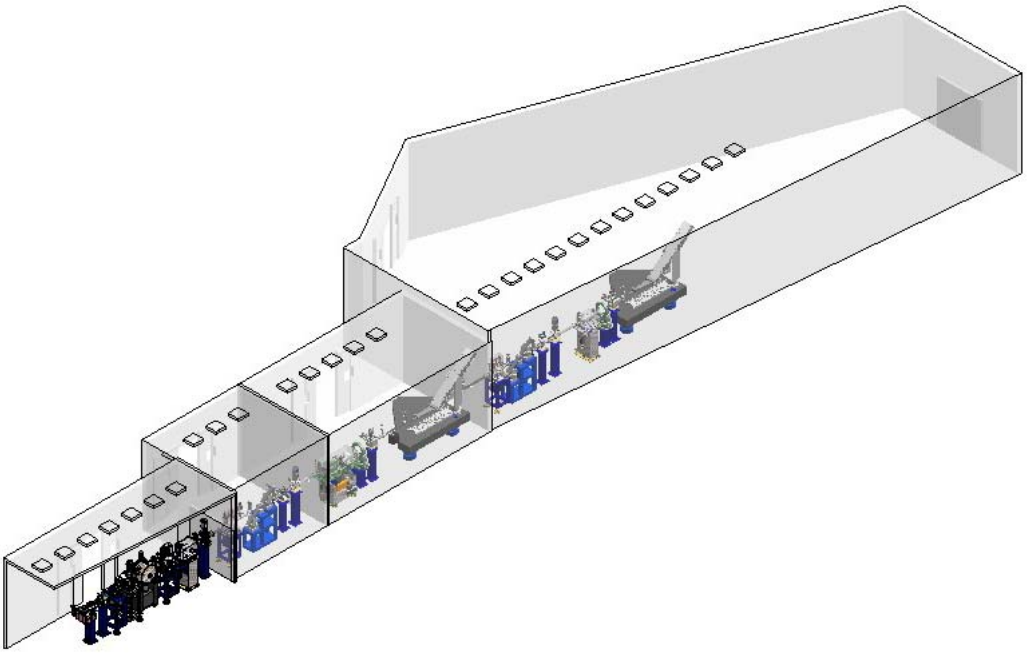

Figure B2. General view of the NSRS-2 IXS beamline and two endstations (In-line HRM) with an in-line, high-resolution monochromator.

1-C Appendix C: List of Key Beamline Components

Table 1.C.1. Proposed beamline layout based on the July 17, 2007 facility numbers.

Beamline Component	Starting position, mm	Length, mm	Vacuum section[1]	Center of Optical Element
Beamline isolation gate valve	26900	70	0/1	
Bellow	26970	175	1	
Pumping Tee	27145	420	1	
Cooled fixed mask	**27565**	**229**	1	**27680**
Bellow	27794	175	1	
CVD Diamond Window	27969	105	1/2	
Bremsstrahlung collimator	28074	388	2	
Bellow	28462	137	2	
Blade BPM	28599	319	2	
Bellow	28918	137	2	
White beam slits	**29055**	**229**	2	**29170**
Cooled Fluorescent screen	29284	211	2	
Bellow	29495	137	2	
Gate valve	29632	70	2/3	
DCM White beam / Bremsstrahlung stop	**29702**	**821**	3	**30113**
Gate valve	30523	70	3/4	
Bellow	30593	137	4	
Quadrant BPM	30730	35	4	
Monochromatic slits Fluorescent screen	30765	553	4	
Bellow	31318	137	4	
Gate valve	31455	70	4/5	
VCM	**31525**	**700**	5	**31875**
Gate valve	32225	70	5/6	
Bellow	32295	200	6	
Monochromatic beam shutter	32495	320	6	
Pipe Hutch Wall at 33.55 m	32815	600 340	6	
ENDSTATION 1				
Bellow	33415	200	6	
Monochromatic slits Fluorescent screen	33615	553	6	
Y-Z profile monitor	34168	406	6	
Bellow	34574	200	6	
Gate valve	34774	70	6/7	
High-resolution monochromator	**34844**	**1031**	7	**35360**
Gate valve	35875	70	7/8	
Bellow	35945	200	8	

Beamline Component	Starting position, mm	Length, mm	Vacuum section[1]	Center of Optical Element
Fluorescent screen	36145	300	8	
Bellow	36445	200	8	
Quadrant BPM	36645	35	8	
Monochromatic beam shutter	36680	320	8	
Pipe Hutch Wall at 37.3 m	37000	680 340	8	
Bellow	37680	200	8	
Gate valve	37880	70		
HFM	**37950**	**900**	8	**38400**
VFM	**38850**	**600**	8	**39150**
Be (150 μm) or SiN window	39450	20	8/9	
Sample position 1 (low vacuum)			9	**39570**
Be (150 μm) or SiN window	39670	20	9/10	
Monochromatic slits	39690	340	10	
Quadrant BPM	40030	35	10	
Bellow	40065	200	10	
Gate valve	40265	70	10/11	
Segmented high-resolution analyser (reflecting back at a different height) Gate valve Bellow/pipe SiN window (200 nm) Strip detector	40335 (finishes at 42835)	2500 70 300 20 600	11	**44238**
Gate valve	42835	70	11/12	
Bellow	43035	200	12	
Pipe Hutch Wall (separating Endstation II) at 46.05 m	43235	17647	12	
ENDSTATION 2 (Backscattering Monochromator option)				
Bellow	60882	200	12	
Gate valve	61082	70	12/14	
Backscattering monochromator	**61152**	**1000**	14	**61652**
Gate Valve	61082	70	14/13	
Bellow	60882	200	13	
Pipe	58932	1950	13	
Bellow	58732	200	13	
Double sided Fluorescent screen	58521	211	13	
Y-Z profile monitor	58115	406	13	
Si table	54415	3700	13	
Gate valve	54345	70	13/15	
Bellow	54145	200	15	
Monochromatic slits Fluorescent screen	53592	553	15	

Beamline Component	Starting position, mm	Length, mm	Vacuum section[1]	Center of Optical Element
Quadrant BPM	53557	35	15	
Bellow	53357	200	15	
VFM	52757	600	15	**53057**[1]
Monochromatic Slits	52692	65	15	
SiN window (200 nm)	52622	70	15	
Sample position 2 (low vacuum) Detector		446 400	16	**52451**[2]
SiN window (200 nm)	52106	70	17	

Notes: 1) Optical distance is 70.247 m from the source.
2) Optical distance is 70.853 m from the source.